Chapter 5

Enhancing Pseudocapacitive Process for Energy Storage Devices: Analyzing the Charge Transport Using Electro-kinetic Study and Numerical Modeling

Fenghua Guo, Nivedita Gupta and Xiaowei Teng

Additional information is available at the end of the chapter

http://dx.doi.org/10.5772/intechopen.73680

Abstract

Supercapacitors are a class of energy storage devices that store energy by either ionic adsorption via an electrochemical double layer capacitive process or fast surface redox reaction via a pseudocapacitive process. Supercapacitors display fast charging and discharging performance and excellent chemical stability, which fill the gap between high energy density batteries and high-power-density electrostatic capacitors. In this book chapter, the authors have presented the current studies on improving the capacitive storage capacity of various electrode materials for supercapacitors, mainly focusing on the metal oxide electrode materials. In particular, the approaches that mathematically simulate the behavior of interaction between electrode materials and charge carriers subject to potentiodynamic conditions (e.g., cyclic voltammetry) have been described. These include a general relationship between current and voltage to describe overall electrokinetics during the charge transfer process and a more comprehensive numerical modeling that studies ionic transport and electrokinetics within a spherical solid particle. The two aforementioned types of mathematical analyses can provide fundamental understanding of the parameters governing the electrode reaction and mass transfer in the electrode material, and thus shed light on how to improve the storage capacity of supercapacitors.

Keywords: pseudocapacitance, diffusion-limited redox process, electrode/electrolyte interface, electrokinetics

1. Introduction

Supercapacitors (SCs), also called electrochemical capacitors, are a class of energy storage devices that store electrical energy by either ionic adsorption via an electrochemical double layer capacitive process or fast surface redox reaction via a pseudocapacitive process. As shown in **Figure 1**, SCs bridge the performance gap between high energy density batteries and high-power-density capacitors (referring to electrostatic capacitors), the two leading electrical energy storage technologies [1]. Batteries technology, especially non-aqueous lithium-ion batteries (LIBs), has been successfully used in various applications in the past two decades especially in consumer electronics and electrical vehicles. On the other hand, capacitive storage technology offers a number of desirable properties hardly found in batteries, including fast charging and discharging process (usually achieved within seconds), long-term cycling life (>10^6 cycles), and high power performance (able to deliver at least 10 times more power than batteries). As a result, capacitive storage technology is very important for applications where a large amount of energy needs to be either stored or delivered quickly, including repetitive conversions between kinetic energy and electric energy (e.g., regenerative braking and forklifting), pulse power applications for laser or radar, power conditioning in the electrical grid to smooth the output of a full or half wave rectifier [2]. It is notable that both capacitive and battery storage technologies have promising applications in stationary storage. Renewable sun and wind energy sources generally have on-peak and off-peak load variations. To accelerate the adoption of renewable energy generation sources, chemical energy storage (e.g., batteries) and capacitive energy storage (e.g., capacitors) are required. Thus, electricity generated during off-peak hours can be stored efficiently and economically for use during peak demand [3].

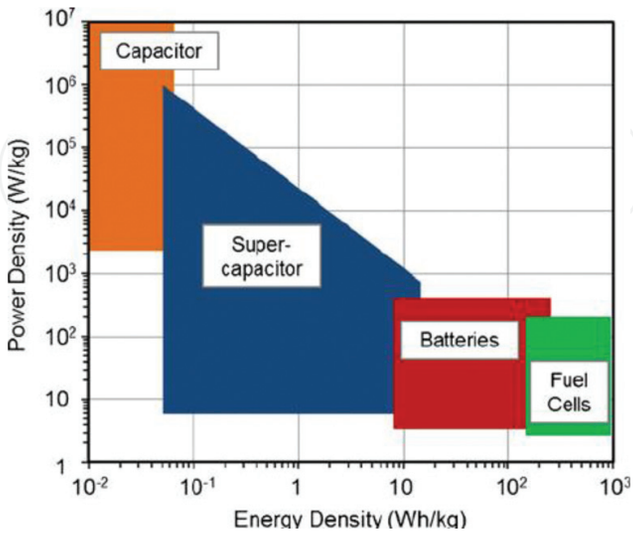

Figure 1. Ragone plot showing supercapacitors are intermediate energy storage devices filling the gap between batteries and conventional capacitors.

Although SCs offer complementary energy storage solution for many applications that are not suitable for batteries, the relatively low storage capacity and energy density limit SCs in more widespread usage. SCs usually contain three general classes of charge storage mechanisms:

- *Electrical double-layer (EDL) capacitive process* relies on the charge separation in a Helmholtz double layer at electrode/electrolyte interface by means of static charge (non-faradaic). The storage capacity of an EDL capacitor can be improved by a large surface area of the electrode/electrolyte interface (most EDL capacitors have a capacitance in a range from 10 to 20 $\mu F/cm^2$). EDL capacitors serve as the basis for the current technology in capacitive energy storage. Carbons are ideal EDL electrode materials for its high electrical conductivity, large surface area, and low density, delivering a storage capacity of up to 150 F g^{-1} in ionic liquid electrolytes [4].

- *Pseudocapacitive process* relies on the charge transfer process primarily happening at the interface between the electrode and the electrolyte. Three faradaic mechanisms have been identified to account for the capacitive electrochemical features that appear in pseudocapacitors, namely, underpotential deposition, redox pseudocapacitance, and intercalation pseudocapacitance [5]. Underpotential deposition typically involves hydrogen atom on the near surface on noble metal oxides (e.g., IrO_2 or RuO_2) [6]. Redox pseudocapacitance occurs at or near the surface of a material, accompanied by adsorption of ions [7]. Intercalation pseudocapacitance occurs when ions intercalate into the channels or layers of a redox-active material accompanied by a faradaic charge-transfer with no crystallographic phase change [8]. Metal oxides, metal carbides or nitrides are ideal pseudocapacitive electrode materials for their reversible redox activity, wide electrochemical potential and high chemical stability [9]. The storage capacity of a pseudocapacitive material is much higher than an EDL capacitive material (the former has a capacitance larger than 100 $\mu F/cm^2$, nearly one magnitude higher than the latter).

- *Diffusion-limited redox process* relies on the kinetically limited intercalation reactions as found in most standard battery materials, where ion intercalation and de-intercalation are intrinsically tied to the slow kinetics of solid phase transition between the intercalated and non-intercalated phases. It is notable that the difference between pseudocapacitive charge storage and battery-like diffusion-limited intercalation is rather vague, especially when the dimensions of an electrode material decreases from the micron-scale down to the nanoscale [10]. At the nanoscale, the specific surface area of a material (overall surface area per unit volume) increases inversely with the size, which results in a significant enhancement of redox pseudocapacitance and intercalation pseudocapacitance. Such enhancement of surface redox (pseudocapacitive) process may become the more dominant charge storage process traditional battery-like intercalation process as the sizes of materials progress from micro-scale to nanoscale. Thus, the materials may evolve from being a typical battery material to a pseudocapacitor material based on their size and/or nanoscale architecture, where phase transition is no longer a distinct structural feature of the electrode materials between the intercalated and non-intercalated states (**Figure 2**).

As discussed above, improving the storage capacity of SCs requires the enhancement of redox processes, such as redox pseudocapacitance, intercalation pseudocapacitance, as well as

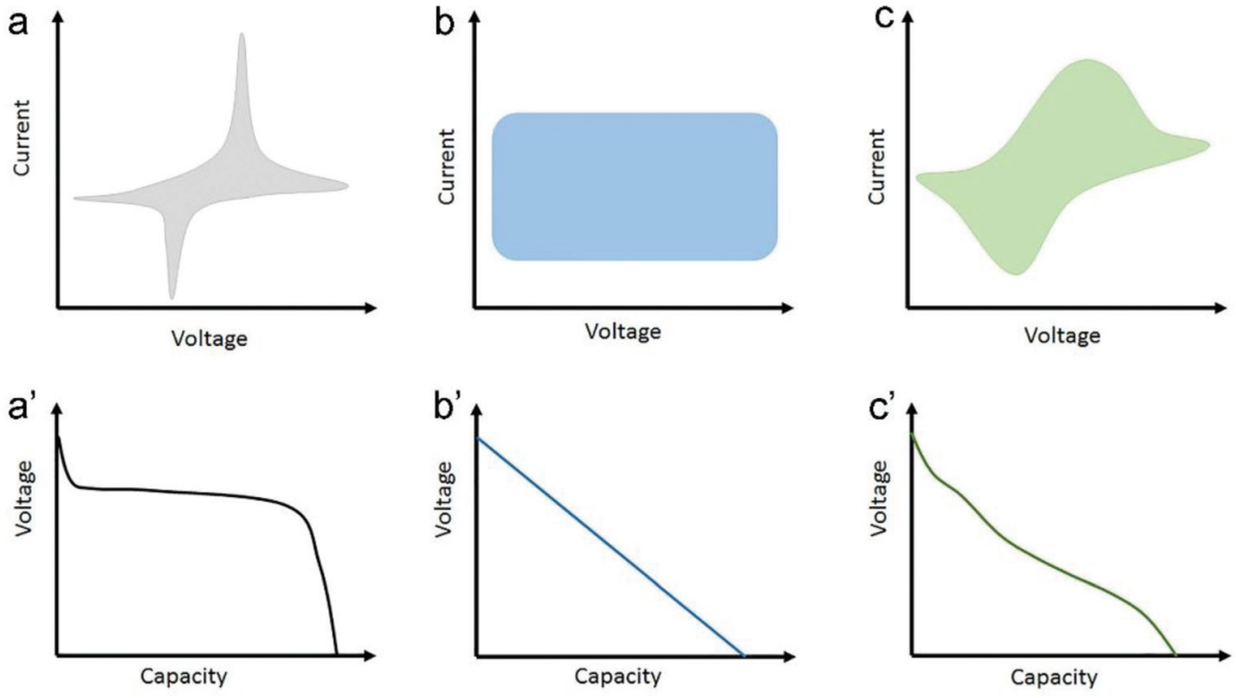

Figure 2. Schematics of charge transfer and storage processes observed in (a, a′) large-sized battery-materials; (b, b′) pseudocapacitive materials, and (c, c′) nano-sized battery-materials.

diffusion-limited redox process. Therefore, the analysis of different charge storage mechanisms also becomes important. The goal of this chapter is thus to examine the parameters (e.g., size, morphology and structure) that will affect the evolution from battery-like behavior to pseudocapacitor behavior and to explore the interplay of these parameters to control redox kinetics.

2. Understanding electrochemical kinetics of charge transfer process by analyzing the electrochemical data during the cyclic voltammetry measurements

Redox reactions involve both surface adsorption/desorption and intercalation/deintercalation of electrolyte cations as shown in Eq. (1):

$$MO_XC \leftrightarrow MO_X + C^+ + e^- \tag{1}$$

where MO is the transition metal oxide and C^+ is the charge carrier (e.g., Li^+, Na^+, or K^+). Upon the incorporation (via intercalation or adsorption) of C^+, M cations will be reduced to balance the charges, and *vice versa*. Moreover, due to the dispersive nature of the electrode composites, separate percolation paths for ion and charge transport may be present, resulting in different paths for long range electronic and ionic conduction. Therefore, influences of the kinetic parameters (e.g., scan rate, potential window) and the structural parameters (e.g., size,

morphology, and crystalline structures) on the redox reactions are crucial to understand the charge-storage mechanism in electrode materials. All the kinetic and structural parameters need to be optimized in order to design cost-effective electrode materials that can store more energy while maintaining a stable electrode/electrolyte interface.

The understanding of the electrokinetics of charge storage inside the metal oxide nanomaterials can be obtained through analyzing the current-voltage curves at various scan rates obtained from CV measurements in the half-cell. The total charge stored in the electrode during SC operation is dependent on a relatively fast surface-controlled capacitive charge storage process and a relatively slow diffusion-controlled redox charge storage process. The latter is promoted by the battery-like intercalation/de-intercalation redox processes of the charge carriers (e.g., Li^+, Na^+), while the former is attributed to the electrical double layer (i.e. EDL capacitance) and pseudocapacitance formed via the separation or adsorption and desorption of charge carriers at the near surface of the electrode.

For a strictly diffusion-limited redox reaction, the rate of charge transfer reactions, namely the current (i_d), is proportional to the square root of the scan rate (v) according to Eq. (2) [11].

$$i_d = 0.495FCA\left(\frac{D\alpha nFv}{RT}\right)^{\frac{1}{2}} \tag{2}$$

$$i_d = k_d v^{0.5} \tag{3}$$

where C is the concentration of charge carriers in the accumulation layer, α is the charge transfer coefficient, D is the diffusion coefficient of the charge carrier inside the electrode materials, n is the number of electrons involved in the Faradaic reaction, A is the surface area of the electrode materials, F is Faraday's constant, R is the molar gas constant, and T is the temperature. Eq. (2) can be further simplified to a form shown in Eq. (3) when all the reaction conditions are fixed except the scan rate.

On the other hand, the capacitive current (i_c) from EDL capacitance and pseudocapacitance has a linear dependence on the scan rate according to Eq. (4):

$$i_c = AC_c v \tag{4}$$

$$i_c = k_c v \tag{5}$$

where C_c is the capacitance from capacitive process and A is a constant. Eq. (4) can be further simplified to a form shown in Eq. (5) when all the reaction conditions are fixed except the scan rate.

Accordingly, the overall current at a given potential can be express as the sum of two separate charge storage mechanisms, that is capacitive current and kinetic current as shown in Eq. (6). Therefore, at higher scan rates, the overall current is dominated by capacitive current (i_c), due to its stronger linear dependence on scan rates shown in Eq. (6), whereas the overall current is dominated by diffusion-limited kinetic current (i_d) at lower scan rates. In this context, the overall current (i_{total}) is usually described by a simple power law as shown in Eq. (7).

$$i_{total} = i_c + i_d = k_c v + k_d v^{0.5} \tag{6}$$

$$i_{total} = a v^b \tag{7}$$

where a is an adjustable parameter and b is a variable heavily dependent on the relative contribution from i_c or i_d. It is apparent that the value of b is equal to either 0.5 or 1 when the overall currents are strictly dominated by capacitive (i_c) or kinetic (i_d) current, respectively.

Figure 3 shows the electrokinetic analysis of aqueous K-ion storage within vanadium oxide nanostructures using cyclic voltammetry (CV) measurements in a three-electrode half-cell with a 1 M KCl electrolyte, where the b-values of the peaks in all three of the color shadowed sections of the anodic and cathodic scans are plotted. In the potential range from −0.1 to 0.3 V (gray region in **Figure 3a**) the K-ion storage in the vanadium oxide is dominated by a diffusion-limited redox process as the b-values for the anodic and cathodic scans are close to 0.5 (b_{anodic} = 0.44, $b_{cathodic}$ = 0.69). In the potential range from 0.7 to 0.9 V (red region in **Figure 3a**) the charge storage process is controlled by surface-related capacitive process because the b-values for the anodic and cathodic scans are very close to 1.0 (b_{anodic} = 0.95, $b_{cathodic}$ = 0.99). While in the potential range from 0.3 to 0.7 V (blue region in **Figure 3a**) both the surface-controlled capacitive and diffusion-limited redox processes contribute to the charge storage as the b-values for the anodic and cathodic scans are between 0.5 and 1.0 (b_{anodic} = 0.81, $b_{cathodic}$ = 0.87). The electrokinetic analysis suggests that charge storage of the vanadium oxide nanostructures benefits from both capacitive and diffusion-limited redox processes. The former process allows the high rate performance and the latter allows the high capacity performance of K-ion storage in the vanadium oxide nanostructures. The contribution of capacitive process (double-layer capacitance and/or pseudo-capacitance) and diffusion-limited redox process to the overall capacity can be quantified with the infinite sweep rate extrapolation, as shown in **Figure 3c**. For example, at a scan rate of 5 mV s^{-1}, 46% of the total capacity is attributed to capacitive process, whereas 93% of the total capacity is attributed to capacitive process at 200 mV s^{-1}.

Moreover, after rearranging Eq. (7) into Eq. (8), the values of k_c and k_d can be determined by the slope and intercepts of the resulting linear function via plotting $i/v^{0.5}$ as a function of $v^{0.5}$ at

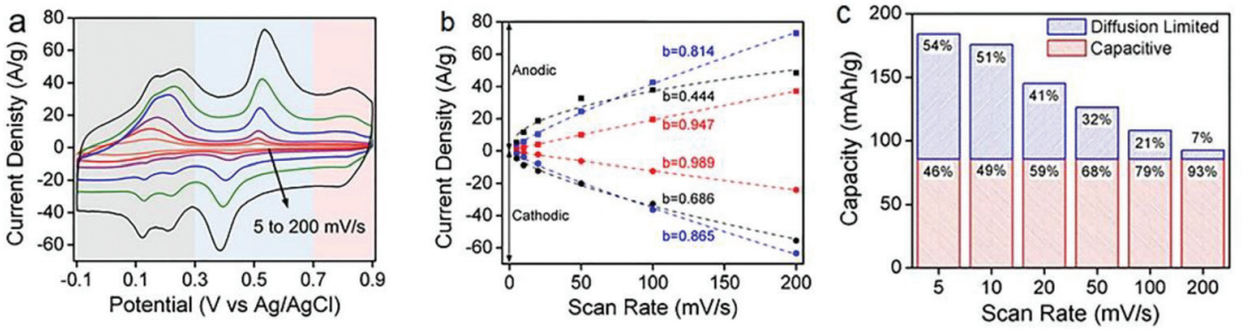

Figure 3. Electrokinetics analysis (b-values) of K-ion storage within the vanadium oxide nanostructures. (a) Cyclic voltammetric curves at various scan rates. (b) The calculated b values during the anodic and cathodic scans. (c) A stacked bar graph showing the percent of total capacitance coming from the diffusion limited and capacitive contributions.

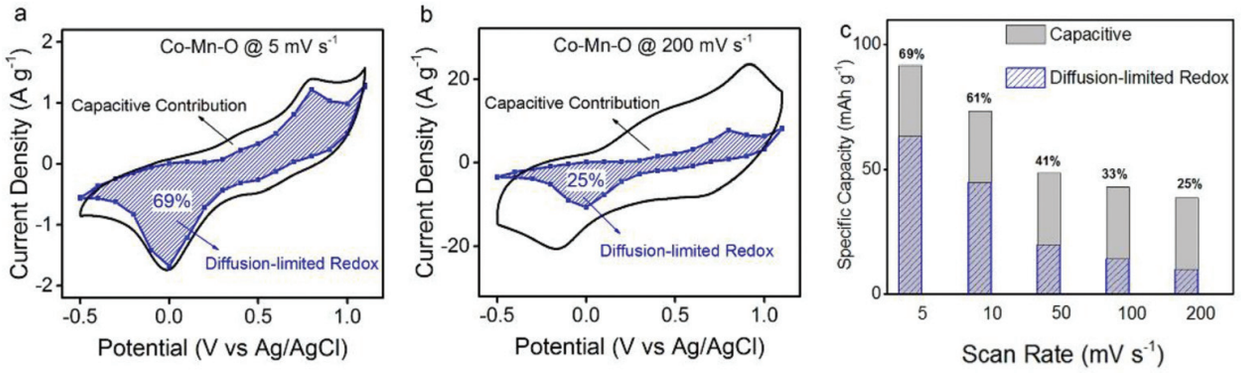

Figure 4. Electrokinetics analysis (k_c and k_d values) of Na-ion storage within the manganese oxide materials. CV current responses of the manganese oxide material are shown at the scan rates of (a) 5 mV s^{-1} and (b) 200 mV s^{-1}. The total current (black line) is obtained experimentally and the diffusion-limited redox current (blue dot line with shadow) is calculated; (c) a stacked bar graph showing diffusion-limited redox capacity and capacitive capacity contribution of the manganese oxide material as a function of scan rate from 5 to 200 mV s^{-1} (diffusion-limited redox capacity contributions are indexed).

various scan rates at a given potential. Therefore, the current attributed to diffusion-limited redox process ($i_d = k_d v^{0.5}$) and capacitive process ($i_c = k_c v$) at each scan rate can be obtained. And thus the potential- and scan rate-dependent charge storage mechanisms (e.g., capacitive or diffusion-controlled redox) during the CV scans can be revealed.

$$i_{total}/v^{0.5} = k_c v^{0.5} + k_d \tag{8}$$

Figure 4a and **b** show the typical CV curves of the manganese oxide material at scan rates of 5 mV s^{-1} and 200 mV s^{-1}, where the distributions of diffusion-limited redox current and capacitive current are calculated and plotted. The complete results of diffusion-limited redox and capacitive contributions of manganese oxide from 5 to 200 mV s^{-1} can be found in **Figure 4c**. It is clear that diffusion-limited redox contributions to the overall charge storage decreased with the increasing scan rate: at low scan rate of 5 mV s^{-1}, diffusion-limited redox process contributed nearly 69% of the overall current, while it only remained 25% at high scan rate of 200 mV s^{-1}. The enhanced capacitive contribution for Na-ion storage found in the manganese oxide material can be attributed to its layered MnO_2 component, where the large interlayer distance (~0.7 nm) facilitates the transport of Na-ion during charge and discharge processes.

3. Understanding electrochemical kinetics of charge transfer process using numerical analysis

Modeling electrodes or full-cells of batteries or supercapacitors has been extensively studied [12–15]. For example, Popov and coworkers have developed a one-dimensional model to analyze the performance of a hybrid system comprised of battery and supercapacitor (based on a Sony 18650 battery and a Maxwell's 10F supercapacitor) under pulse discharge currents

[15]. The proposed model has not only successfully predicted the power-energy relationship compared with the practical experimental conditions, but also reveals the capability of the hybrid system to deliver higher energy density than the battery-alone system while operating at high power density. However, little has been done on simulating the transition of the electrochemical behavior between the battery-type and capacitor-type charge storage mechanisms. In this book chapter, we present numerical solutions for a simple model of an electrode material and discuss in detail the interplay between redox reaction and diffusion of charge carriers, as well as the effect of dependence of open-circuit-voltage on chemical composition on the overall cyclic voltammetry behavior of the electrode in a half-cell setting. We are able to show the transition from a diffusion-limited charge transfer process (battery-like electrochemical behavior) to kinetic-limited charge transfer process (capacitor-like behavior) by changing the structural and experimental conditions.

3.1. The description of the mathematical model

Figure 5 shows a schematic of a single spherical electrode material model. The following assumptions are made during the analysis:

i. The particle is a perfect solid sphere.

ii. The transport of charge carriers (cations) within the solid particle is only limited by diffusion, and only radial diffusion has been considered. It is also assumed that the potential gradient within the particle is negligible, and thus migration of cations does not occur.

iii. The charge-transfer reaction is governed by the Butler-Volmer electrokinetic expression.

Therefore, the flux of charge carriers ($\boldsymbol{N}$) within the particle can be described using Eq. (9), and mass conservation of the charge carriers in the particle can be described using Eq. (10)

$$\boldsymbol{N} = -D\nabla c \tag{9}$$

$$\frac{\partial c}{\partial t} = -\nabla \cdot \boldsymbol{N} \tag{10}$$

where c is the concentration of charge carriers (such as Li^+ or Na^+), D is the diffusion coefficient during the ionic transport within the particle (assumed to be a constant).

Combining Eqs. (9) and (10) gives the conservation of the charge carriers in spherical coordinates:

$$\frac{\partial c}{\partial t} = D\left(\frac{\partial^2 c}{\partial r^2} + \frac{2}{r}\frac{\partial c}{\partial r}\right) \tag{11}$$

Starting from certain discharged state with a homogenous concentration of the charge carriers (c_0) in the particle, the electrokinetics during charging (oxidation or extraction of charge carriers out of the particle) and discharging (reduction or insertion of charge carriers into the

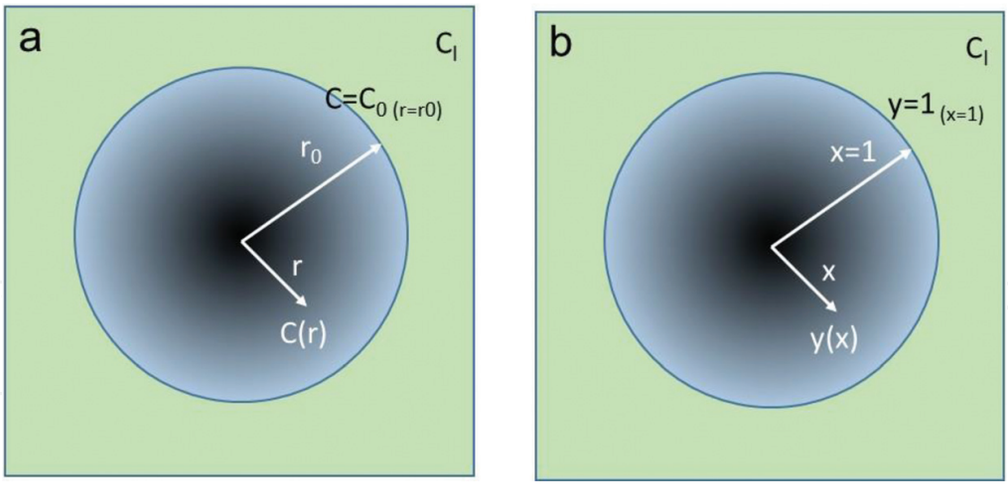

Figure 5. Schematic of a single spherical electrode material model in (a) a regular parameter denotation and (b) a dimensionless parameter denotation (when $c_0 = c_t$).

particle) processes can be described by a partial differential equation (Eq. (11)) with a set of initial condition (Eq. (12)) and boundary conditions at the surface of the particle (Eqs. (13) and (17)) and at the center of the particle (Eq. (14)):

$$c(r, t = 0) = c_0 \tag{12}$$

$$\frac{i}{F} = -D\left(\frac{\partial c}{\partial r}\bigg|_{r=r_0}\right) \tag{13}$$

$$\frac{\partial c}{\partial r}\bigg|_{r=0} = 0 \tag{14}$$

where i is the current density at the electrode surface and r_0 is the radius of the particle.

It is notable that the current density at the surface is also governed by the Butler-Volmer equation:

$$\frac{i}{F} = k(c_l)^{1-\beta}(c_\theta)^{1-\beta}(c_s)^{\beta}\left\{\exp\left(\frac{(1-\beta)F\eta}{RT}\right) - \exp\left(-\frac{\beta F\eta}{RT}\right)\right\} \tag{15}$$

where k is a reaction rate constant, C_l is the concentration of the charge carrier in the liquid phase (assumed to be a constant in the calculation), c_θ is the surface concentration of vacant sites ready for cation intercalation, c_s is the concentration of cation on the surface of the electrode, and c_t is the concentration of total sites for seating cations ($c_\theta = c_t - c_s$). R is the gas constant, T is the temperature, and β is the symmetry factor, representing the fraction of the electrical potential used to promote the cathode reaction (β is usually considered to be 0.5). The overpotential η is defined as the difference between the applied potential (U_{app}) and the open-circuit potential of the particle (U) as shown in Eq. (16). It is assumed that U_{app} is uniform throughout the particle.

$$\eta = U_{app} - U \tag{16}$$

Combination of Eqs. (13) and (15) gives the following equation:

$$-D\left(\left.\frac{\partial c}{\partial r}\right|_{r=r_0}\right) = k(c_l)^{1-\beta}(c_\theta)^{1-\beta}(c_s)^{\beta}\left\{\exp\left(\frac{(1-\beta)F\eta}{RT}\right) - \exp\left(-\frac{\beta F\eta}{RT}\right)\right\} \tag{17}$$

To facilitate the numerical analysis, the partial differential equation with its initial condition and boundary conditions as shown from Eqs. (11)–(17) can be transformed into dimensionless form with the following dimensionless variables:

i. dimensionless time $\tau = \frac{tD}{r_0^2}$

ii. dimensionless distance from the particle center $x = \frac{r}{r_0}$

iii. dimensionless concentration $y = \frac{c}{c_t}$

iv. dimensionless current density $j = \frac{ir_0}{FDc_t}$

Eqs. (11)–(14) then become following expressions accordingly:

$$\frac{\partial y}{\partial \tau} = \frac{\partial^2 y}{\partial x^2} + \frac{2}{x}\frac{\partial y}{\partial x} \tag{18}$$

$$y(x,0) = 1(when\ c_0 = c_t) \tag{19}$$

$$j = -\left(\left.\frac{\partial y}{\partial x}\right|_{x=1}\right) \tag{20}$$

$$\left.\frac{\partial y}{\partial x}\right|_{x=0} = 0 \tag{21}$$

Eq. (19) is applicable only when ($c_0 = c_t$), while here we assume c_0 is lower but near c_t ($y < 1$) and the electrochemical process starts from the oxidation of the particles (extraction of charge carriers from the solid particles as shown in the forward direction in Eq. (1)), Eq. (17) then becomes:

$$\left.\frac{\partial y}{\partial x}\right|_{x=1} + a\left(y|_{x=1}\right)^{\beta}\left(1 - y|_{x=1}\right)^{1-\beta}\left\{\exp\left(\frac{(1-\beta)F(U_{app}-U)}{RT}\right) - \exp\left(-\frac{\beta F(U_{app}-U)}{RT}\right)\right\} = 0 \tag{22}$$

where $y|_{x=1} = c_s/c_t$ and $a = \frac{kr_0 c_l^{1-\beta}}{D}$.

Under potentiodynamic simulation, the applied potential changes linearly with time

$$U_{app} = U_0 + vt \tag{23}$$

where U_0 is the initial applied potential, v is the potential sweep rate.

Eqs. (18)–(23) can be solved with a partial differential equation solver PDE2D using the parameters listed in **Table 1**.

3.2. The influence of open-circuit voltage on the electrochemical behavior

From the numerical analysis, we have found that the value of the OCV of the particles at different concentration of the charge carriers strongly affects the shape of the CV, and therefore the entire charge storage mechanism. In this study, two different open-circuit voltage (OCV) expressions (as a function of the concentration of the charge carrier in the particle) are used as shown in **Figure 6**. They include (i) the simplified OCV of a capacitor material (**Figure 6a**), where the OCV linearly decreases with increasing concentration of charge carrier within the particle; (ii) the simplified OCV of a Li-ion battery material during phase transition (**Figure 6b**), where OCV of the particle is nearly independent of the charge carrier concentration within the particle for most of the composition range.

Considering one-electron transfer and the insertion of the charge carrier into the solid spherical particles occurs as shown in Eq. (24).

$$MO_X + C^+ + e^- \leftrightarrow MCO_X \tag{24}$$

We assume that the conversion of MO_X into MCO_X is a one-phase reaction, where MO_X and MCO_X have a similar solid-solution type structure, analogous to proton intercalation into RuO_2 materials. The degrees of freedom can be calculated by the Gibbs phase rule:

$$F = C - P + 2 \tag{25}$$

where F is the degree of freedom, which is the number of thermodynamic parameters necessary for defining a system, C is the number of components, and P is the number of phases. For the reaction shown in Eq. (24), the system has two components (C = 2) including the charge carriers (C^+) and the host particle (MO_X), the degree of freedom is equal to 3 (F = 2 − 1 + 2 = 3). Beside the two intensive parameters, usually pressure and temperature, there is one additional degree of freedom that needs to be specified for the system. Thus, the chemical potential of the electrode (or OCV) has to be a function of temperature, pressure, and composition (the concentration of the charge carriers in the particle). Once composition changes (as the last degree

D ($cm^2\ s^{-1}$)	10^{-9}
β	0.5
c_l ($mol\ dm^3$)	1.0
r_0 (cm)	5×10^{-4}
K ($cm^{5/2}\ s^{-1}\ mol^{-1/2}$)	6.3×10^{-5}
V ($V\ s^{-1}$)	10^{-4}
a (dimensionless)	1

Table 1. Parameters set for the calculation.

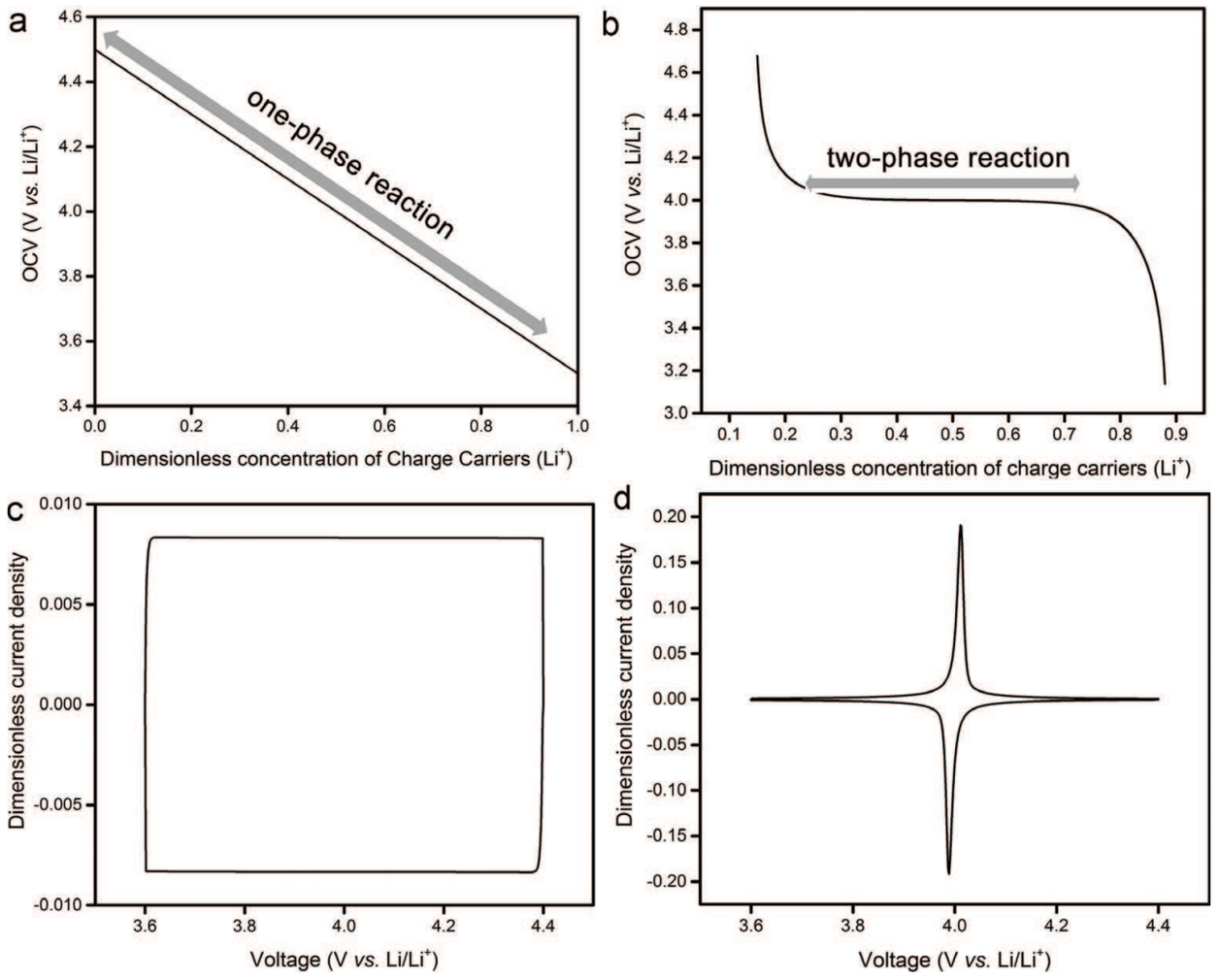

Figure 6. Simulated open-circuit-voltage (OCV) as a function of concentration of charge carrier (Li^+) in (a) one-phase reaction and (b) two-phase reaction, and (c and d) their corresponding CVs curves.

of freedom), the OCV of the host particle changes accordingly at fixed temperature and pressure, as shown in **Figure 6b**. Therefore, in the one-phase discharge reaction (Eq. (24)), the voltage changes linearly with the concentration of the charge carriers.

As C^+ continuously inserts into MCO_X, the further reduction of M cation eventually leads to the formation of new M-containing species (now it becomes a two-phase reaction), resulting in a new degree of freedom of 2 ($F = 2 - 2 + 2 = 2$). For a fixed pressure and temperature, there is no more independent degree of freedom left and all the thermodynamic functions including OCV should remain constant once the composition changes. Therefore, as shown in **Figure 6a** in the two-phase discharge reaction, the OCV is constant with the concentration of the charge carrier.

It is clear that in a two-phase reaction (**Figure 6d**), the CV curves show the distinct redox features that represent conventional battery material behavior. This is also congruent with the fact that a typical battery intercalation/deintercalation reaction is accompanied with a phase transition. On the other hand, in a one-phase reaction (**Figure 6c**), the CV curve shows a square-shaped current versus potential plot without distinct redox features. This unique CV

shape is often observed in classic EDL capacitor that uses carbon as electrode material or pseudocapacitor that uses RuO_2 as electrodes and H_2SO_4 as electrolyte. This simulation again highlights the fundamental difference between a battery material and a capacitor material: the former undergoes a phase transition upon the interaction with cation, while the latter can interact with cation without generation of a new crystalline phase.

3.3. The influence of interfacial reaction and diffusion of charge carriers on the electrochemical behavior

Parameter a is the dimensionless factor (shown in Eq. (22)) involving the concentration of the charge carriers in the liquid phase, and can be considered as the ratio of interfacial reaction rate ($kc_l^{2-\beta}$) to the diffusion rate of the charge carriers on the surface of the particle (Dc_l/r_0) as shown in Eq. (26).

$$a = \frac{kr_0 c_l^{1-\beta}}{D} = \frac{kc_l^{2-\beta}}{Dc_l/r_0} \tag{26}$$

A large value of a indicates a faster interfacial charge-transfer kinetics and a slower diffusion of charge carrier, usually resulting from a large rate constant (k), a large particle radius (r_0) or a small diffusion coefficient (D). **Figure 7** shows the simulated CVs for various values of a at the scan rate of 0.1 mV/s, in which all the parameters described in the definition of a are fixed except the value of k. It is clear that the shapes of the CV are strongly dependent on the value of a. When the values of a increases, the peak potential of the anodic scan (oxidation reaction) shifts to lower potential values with a relatively narrower peak. Similarly, the peak potential of

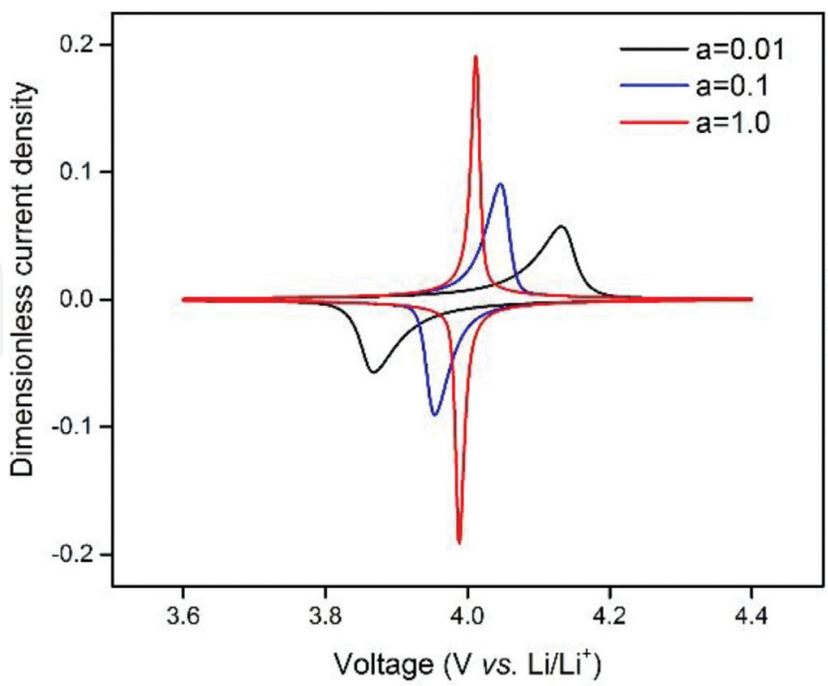

Figure 7. Simulated CV curves as a function of parameter a.

the cathodic scan (reduction reaction) shifts to higher potential values with a narrower peak. These changes strongly suggest that a large value of a reflects a fast interfacial reaction and/or a slow diffusion. Therefore, the extraction (anodic scan) and insertion (cathodic scan) of the charge carriers are limited by diffusion of charge carriers in the solid spherical particle, probably attributed to a relatively low diffusion coefficient (D) and/or a large particles size (r_0). Accordingly, at a large value of a, the solid particle behavior is closer to a battery electrode material, where diffusion-limited charge transport is the slowest step during the electrochemical process. In this context, to increase the capacitive charge transfer contribution, a smaller sized electrode and an electrolyte with cations having a higher diffusivity in the host electrode material is needed. The former points to the synthesis of nanostructured electrode material and the latter indicates Li-containing electrolyte. It is also notable that since the value of β is between 0 and 1, the value of $(1 - \beta)$ is always higher than zero. Therefore, it indicates that a low electrolyte concentration favors the contribution of capacitive process, though the overall charge storage might decrease.

Acknowledgements

This work was supported by the US Department of Energy (DOE), Office of Science, Basic Energy Sciences under Award # DE-SC0010286 (XT, FG). The work on synchrotron test is also supported by the National Science Foundation under Award #147791(FG).

Author details

Fenghua Guo, Nivedita Gupta and Xiaowei Teng*

*Address all correspondence to: xw.teng@unh.edu

Department of Chemical Engineering, University of New Hampshire, Durham, New Hampshire, USA

References

[1] Conway BE. Transition from supercapacitor to battery behavior in electrochemical energy-storage. Journal of the Electrochemical Society. 1991;**138**:1539-1548

[2] Burke A. Ultracapacitor technologies and application in hybrid and electric vehicles. International Journal of Energy Research. 2010;**34**:133-151

[3] Turner JA. A realizable renewable energy future. Science. 1999;**285**:687-689

[4] Simon P, Gogotsi Y. Materials for electrochemical capacitors. Nature Materials. 2008;**7**: 845-854

[5] Conway BE, Birss V, Wojtowicz J. The role and utilization of pseudocapacitance for energy storage by supercapacitors. Journal of Power Sources. 1997;**66**:1-14

[6] Zheng JP, Cygan PJ, Jow TR. Hydrous ruthenium oxide as an electrode material for electrochemical capacitors. Journal of the Electrochemical Society. 1995;**142**:2699-2703

[7] Wei WF, Cui XW, Chen WX, Ivey DG. Manganese oxide-based materials as electrochemical supercapacitor electrodes. Chemical Society Reviews. 2011;**40**:1697-1721

[8] Augustyn V et al. High-rate electrochemical energy storage through Li^+ intercalation pseudocapacitance. Nature Materials. 2013;**12**:518-522

[9] Arico AS, Bruce P, Scrosati B, Tarascon JM, Van Schalkwijk W. Nanostructured materials for advanced energy conversion and storage devices. Nature Materials. 2005;**4**:366-377

[10] Gogotsi Y, Simon P. True performance metrics in electrochemical energy storage. Science. 2011;**334**:917-918. DOI: 10.1126/science.1213003

[11] Conway BE. Electrochemical Supercapacitor: Scientific Fundamental and Technological Applications. Kluwer Academic/Plenum Publisher; 1999

[12] Zhang D, Popov BN, White RE. Modeling lithium intercalation of a single spinel particle under potentiodynamic control. Journal of the Electrochemical Society. 2000;**147**:831-838

[13] Chandrasekaran R, Magasinski A, Yushin G, Fuller TF. Analysis of lithium insertion/deinsertion in a silicon electrode particle at room temperature. Journal of the Electrochemical Society. 2010;**157**:A1139-A1151

[14] Doyle M, Newman J, Gozdz AS, Schmutz CN, Tarascon JM. Comparison of modeling predictions with experimental data from plastic lithium ion cells. Journal of the Electrochemical Society. 1996;**143**:1890-1902

[15] Sikha G, White RE, Popov BN. A mathematical model for a lithium-ion battery/electrochemical capacitor hybrid system. Journal of the Electrochemical Society. 2005;**152**:A1682-A1693

IntechOpen